


FULL PAPER

Open Access



# Cause of destructive strong ground motion within 1–2 s in Mukawa town during the 2018 $M_w$ 6.6 Hokkaido eastern Iburi earthquake

Nobuo Takai<sup>1\*</sup> , Michiko Shigefuji<sup>2</sup>, Jun Horita<sup>3</sup>, Shingo Nomoto<sup>3</sup>, Takahiro Maeda<sup>4</sup>, Masayoshi Ichiyanagi<sup>5</sup>, Hiroaki Takahashi<sup>5</sup>, Hiroaki Yamanaka<sup>6</sup>, Kosuke Chimoto<sup>6</sup>, Seiji Tsuno<sup>7</sup>, Masahiro Korenaga<sup>7</sup> and Nobuyuki Yamada<sup>8</sup>

## Abstract

We investigated the cause of destructive ground motion during the 2018 Hokkaido eastern Iburi earthquake. We conducted strong motion observations of aftershocks and microtremors and the surface wave method in the damaged areas of the town of Mukawa, Hokkaido prefecture, Japan. The ground accelerations were continuously recorded during a period of approximately 3 months after the main shock on September 6, 2018. The heavily damaged buildings were mainly situated around the strong motion station (HKD126) in Mukawa town. Such concentration of damage can be explained by the strong power that was observed in the 1–2 s period of the response spectrum at this station. We estimated the S-wave velocity profiles of this station site and a temporary station site that was installed on a nearby hill. The estimated S-wave velocity, which was inverted from phase velocity structures with the microtremor array and the surface wave method observations explained the difference in the SH-wave amplification characteristics between the two sites. An analysis of HKD126 and the temporarily observed records clearly indicates the strong effects of the local geological conditions on the heavily damaged area of Mukawa. The strong ground motion power generated during the main shock in Mukawa for 1–2 s period was mainly amplified by this shallow underground velocity structure.

**Keywords:** The 2018 Hokkaido eastern Iburi earthquake, Strong ground motion, Velocity structure, Temporary strong motion observation, Microtremor measurement, Multichannel analysis of surface wave, S-wave velocity, Site amplification

## Introduction

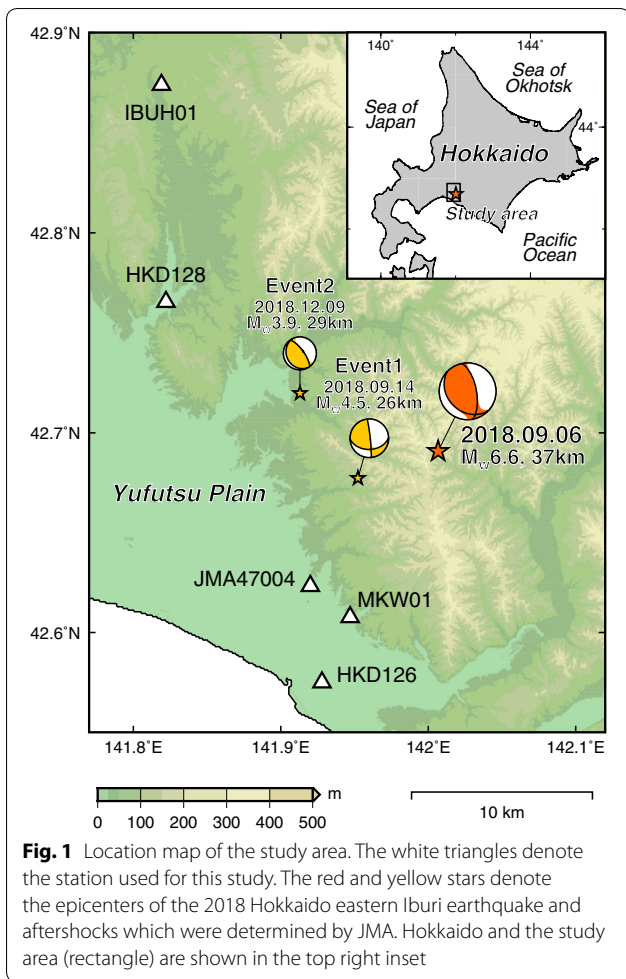
The Hidaka mountain range in central Hokkaido, Japan, is formed by the Hidaka arc–arc collision zone (e.g., Iwasaki et al. 2004), with the eastern boundary fault zone of Ishikari lowland on the west side and the Tokachi plain fault zone on the east side. The 2018 Hokkaido eastern Iburi earthquake ( $M_w$  6.6) occurred at 03:08 JST on September 6, 2018, in this arc–arc collision zone. The Japan Meteorological Agency (JMA) magnitude ( $M_{JMA}$ ) was 6.7, and the hypocentral depth was 37 km. The maximum JMA seismic intensity of 7 was observed in Atsuma town. During this earthquake, 41 people died mainly owing to

a large landslide in Atsuma town. Several buildings damaged by the strong ground motion were mainly concentrated around the Mukawa district in Mukawa town. At the Kyoshin network (K-NET) Mukawa (HKD126) and JMA Atsuma Shikanuma (JMA47004) strong motion stations, the strong motion records indicated a strong power that was able to destroy timber frame buildings. It is important to investigate the cause of such dangerous ground motion despite a not shallow and moderate-sized earthquake.

In this study, we focused on the cause of the strong ground motion characteristics of HKD126. Therefore, we examined the difference in the velocity structures of HKD126 and a temporary station “MKW01” that was installed on a hill close to HKD126. To analyze the velocity structures, temporary strong motion observations,

\*Correspondence: tki@eng.hokudai.ac.jp

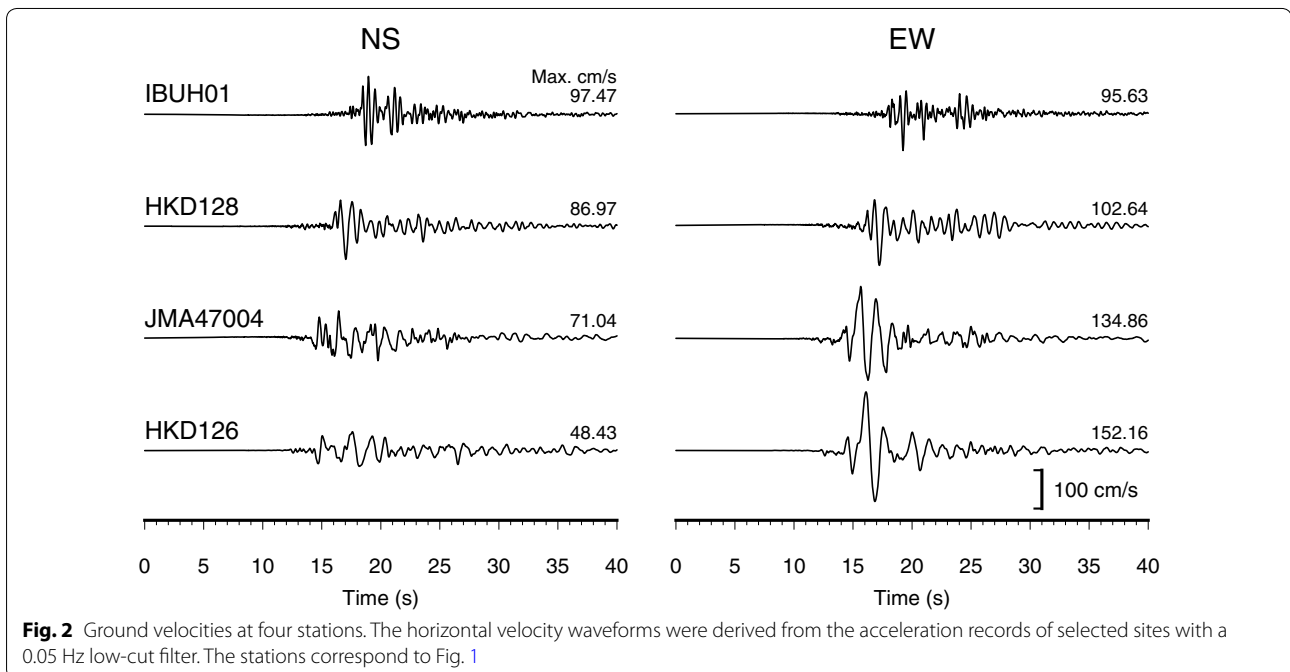
<sup>1</sup> Hokkaido University, Kita 13, Nishi 8, Kita-ku, Sapporo, Hokkaido, Japan  
Full list of author information is available at the end of the article

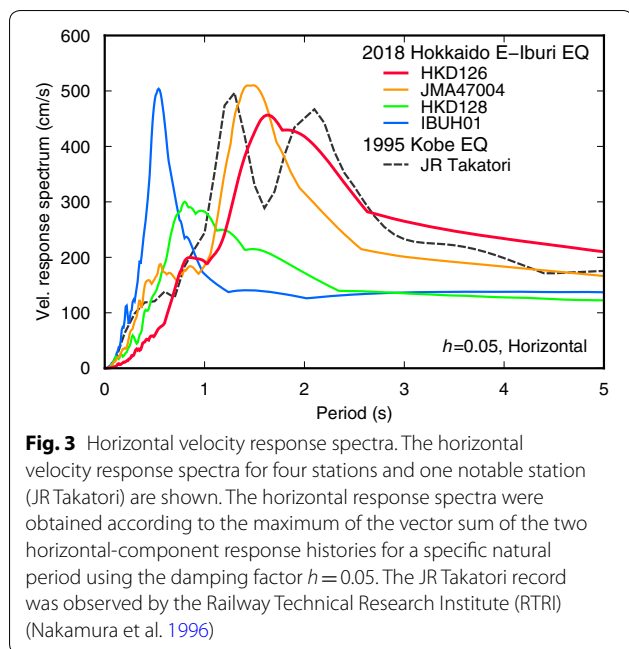


microtremor array observations, and multichannel analysis of the surface wave method (MASW) with an active source were carried out. Furthermore, the strong motion amplification characteristics were discussed with estimated S-wave velocities ( $V_s$ ).

### Features of strong ground motions around the epicentral area

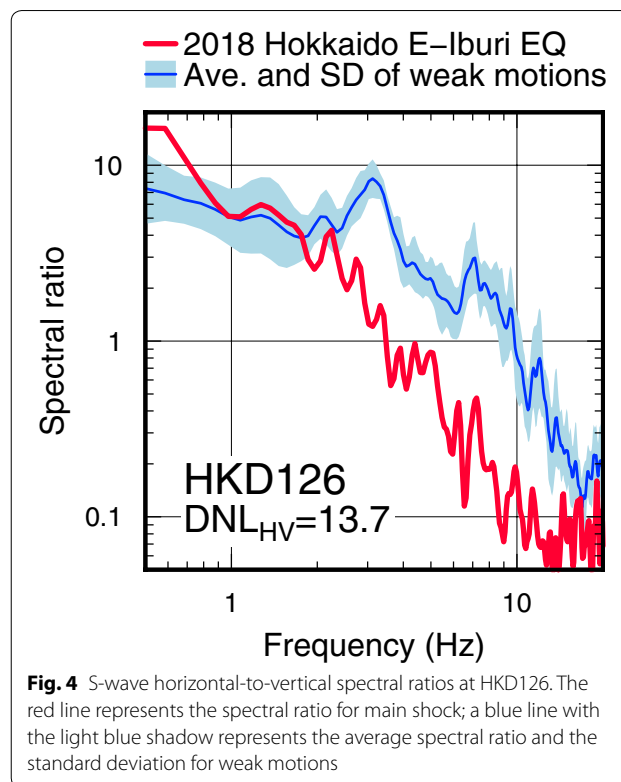
We selected stations around the epicentral area (Fig. 1). The horizontal velocity waveforms derived from acceleration records are shown in Fig. 2. It can be clearly seen that the 1–2 s period waves are included in the waveforms at JMA47004 and HKD126. We calculated the horizontal velocity response spectra ( $h=0.05$ ); the horizontal response spectrum was obtained using the maximum of the vector sum of the two horizontal-component response histories for a specific natural period. These horizontal velocity response spectra of the main shock recorded at four epicentral stations are compared with that of the 1995 Kobe earthquake at JR Takatori station (Hyogo-prefecture: Nakamura et al. 1996), as shown in Fig. 3. The velocity response at HKD126 and JMA47004 indicate that the range of 1–2 s period is dominated. The response spectra of the Kiban Kyoshin network (KiK-net) Oiwake (IBUH01) and K-NET Hayakita (HKD128) are completely different from those of HKD126 and JMA47004. These records at the northern stations IBUH01 and HKD128 are dominated by a shorter period, around the range of 0.5–1.0 s (Fig. 3). We further investigated the difference in the amplitude of the horizontal





components of the velocity waveforms at HKD126 and JMA47004 (Fig. 2); the EW components amplitude are larger than the NS components. These stations are located near the nodal plane of the focal mechanism; therefore, the difference may be owing to the radiation patterns of the seismic source. In general, strong ground motions are affected by the nonlinear response of the surface soft soil. The strong motion record of HKD126 was examined in terms of the nonlinear effects using the degree of nonlinear effect (DNL) method (Noguchi and Sasatani 2008). The DNL was calculated using the horizontal to vertical Fourier spectral ratio of weak motion records and the strong motion one of the surface records for 10.24 s of the S-wave part (Noguchi and Sasatani 2008). The DNL value (Fig. 4) was 13.7, which indicates that large nonlinearity occurred by the threshold DNL value of 4 (Noguchi et al. 2016). The predominant period of 1–2 s might have changed from the short-period side owing to this large nonlinearity.

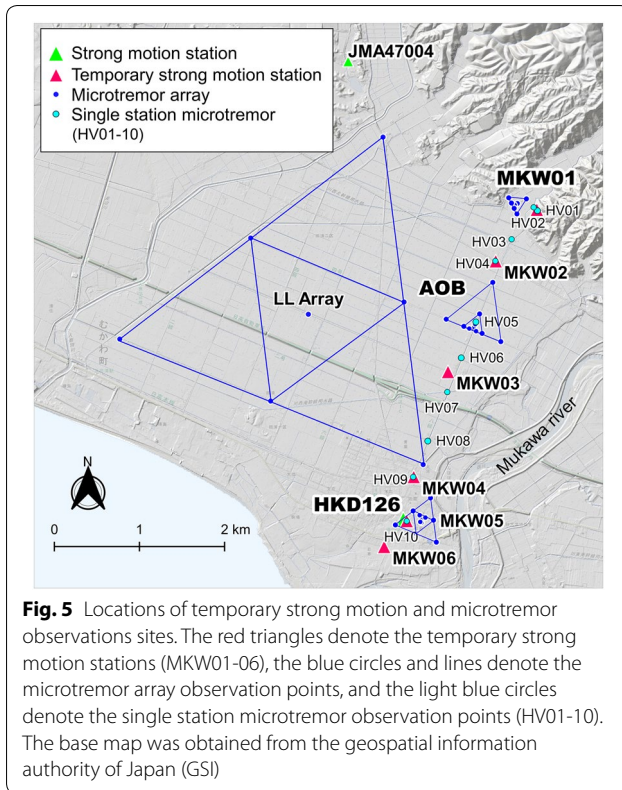
Minor building damage occurred over a wide area, including the Sapporo metropolitan area. However, the heavy damage of the timber frame buildings that were destroyed by the strong ground motion was directly concentrated in the Mukawa district of Mukawa town. We could not determine the building damage clearly around JMA47004 because there were few buildings around this station. HKD126 is located near the heavily damaged area. From previous studies, it is clear that the 1–2 s periods have a potential influence on the timber frame building damage (e.g., Sakai et al. 2004). The response spectrum of the JR Takatori station record which has



JMA seismic intensity of 7 was known as the *Damage belt* (e.g., Kawase 1996) during the 1995 Kobe earthquake. From this comparison, we can observe that the records at HKD126 and JMA47004 have dominated period ranges of 1–2 s similar to the record at JR Takatori.

**Characteristics of strong ground motions at HKD126 and MKW01 stations**

We installed a seismometer at a hill to know the effect of the surface geology at HKD126 on the strong ground motion. The Headquarters for Earthquake Research Promotion (2018) provide site amplification factors, for example, engineering geomorphologic classification and  $AVS_{30}$  (average S-wave velocity in the upper 30 m) in the Japan Seismic Hazard Information Station (J-SHIS). A black marsh, delta and coastal lowland, natural levee, and abandoned river channel of the engineering geomorphologic classification are distributed around HKD126 site. We considered this classification to select the site of a temporary station at a hill in Mukawa town (MKW01), which was located approximately 4 km north from the HKD126 (Fig. 5). The observation was carried out from September 10, 2018, to December 16, 2018, for approximately 3 months. The seismometers used are an over dumping moving coil type accelerometer (Mitutoyo JEP-6A3 2 V/g). The data loggers are 24-bit (Hakusan LS-8800) in 100 Hz sampling with 12 V load batteries.



The internal clock signal of each instrument was calibrated with a GPS timing signal every 1 h. The sensor was fixed with a two-pack type epoxy-based adhesive on the paved road. The photograph of the setup is shown in Fig. 6. The velocity waveforms and acceleration Fourier spectra of the  $M_w$  4.5 (September 14, 2018, Event 1 in Fig. 1) aftershock at the two stations HKD126 and

MKW01 are shown in Fig. 7. We observed a significant difference in the amplitudes of the waveforms, spectral amplitudes, and predominant frequency of the spectra. The differences between the NS and EW components were affected by the source wave radiation pattern similar to those for the main shock.

The significant differences of these near two sites necessitate the estimation of the velocity structures of both sites, which will reveal the cause of the destructive strong ground motion during the main shock at HKD126.

### Estimation of S-wave velocity structures

We present the details regarding the methods for exploring and the results of the estimation of the  $V_s$  structures in this section.

#### Methods

To determine the difference in waveforms recorded at HKD126 and MKW01, we performed microtremor array (radii = 40–2000 m) observations at three sites around HKD126. To determine the variety of the engineering bedrock depth, we selected another site Aoba (AOB) as the mid-point between HKD126 and MKW01; the locations of these three sites are indicated in Fig. 5. We used servo-type velocity seismometers (Lennertz Le-3D/5 s) and 24-bit data loggers (Hakusan LS-7000XT) set in 100 Hz sampling with GPS time calibration. The locations of the observation sites and array sizes are summarized in Table 1. The example of the measurement setup is shown in Fig. 6. We selected the low noise section from the entire data to examine the phase velocities of Rayleigh waves using the spatial autocorrelation (SPAC) method (Okada 2003). Furthermore, we used small arrays (radius = approximately 1–7 m) at HKD126;



**Fig. 6** Photographs of the setting situation. The temporarily strong motion station (left: MKW01). The microtremor observation (right)

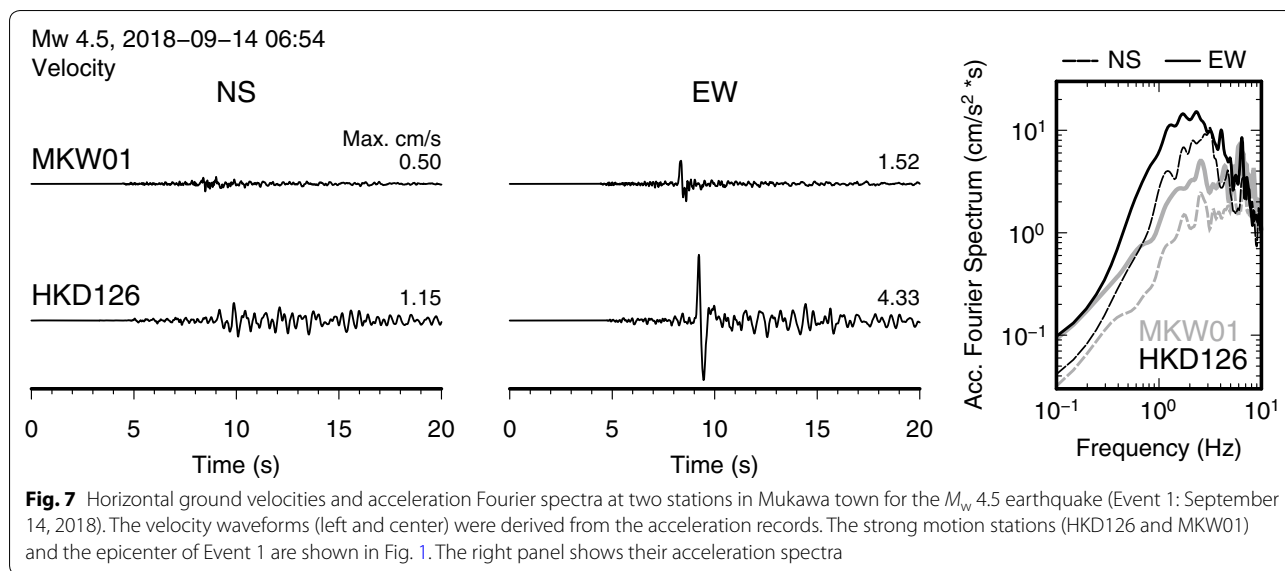


**Table 1** Array sizes and locations for the microtremor array observations

Code	Array sizes (m)		Center location	
			Lat. (°N)	Lon. (°E)
LL	–	$R=2240, 1120$	42.59665	141.91430
MKW01	M	$R=120$	42.60834	141.94421
	S	$R=40$	42.60816	141.94379
	SS1	$R=6.9, 3.5$	42.60740	141.94751
	SS2	$R=2.3, 1.2$	42.60740	141.94751
AOB	L	$R=400$	42.59669	141.93881
	M	$R=133$	42.59464	141.93917
	S	$R=50$	42.59521	141.93795
HKD126	LM	$R=300, 150$	42.57469	141.93047
	S	$R=40$	42.57510	141.93055
	SS1	$R=6.9, 3.5$	42.57464	141.92825
	SS2	$R=2.3, 1.2$	42.57464	141.92825

for this case, we used an over dumping moving coil accelerometer (Mitutoyo JEP-6A3 2 V/g). The large array (LL: radius=2000 m) phase velocity data were used for the three sites, as we could not set up the large array for the sites. This assumption of the common use for all site is obtained from the low variations of seismic bedrock depth in J-SHIS on this area. And phase velocities of the large array (L: radius=400 m) at AOB were used for the MKW01 estimation.

We also carried out MASW on the high-frequency phase velocity at HKD126 and MKW01. We set 24 geophones of 4.5 Hz vertical component spaced 1 m apart with GEODE (Geospace Technologies) and an 8 kg wood

hammer. The phase velocities of MASW were examined by the frequency-wave number method (e.g., Park et al. 1999). The phase velocities determined using MASW in the high-frequency range were combined with the phase velocities determined using the SPAC method in the low-frequency range (Fig. 8).

There are existing models for this area: the Japan Seismic Hazard Information Station (Fujiwara et al. 2012) version 2 model (J-SHIS V2), the Geological Survey of Japan, the National Institute of Advanced Industrial Science and Technology (AIST) model (Yoshida et al. 2007), and the Hatayama et al. (2007) model. First, we examined the underground  $V_s$  structure at HKD126 with the observed phase velocity from the SPAC and MASW methods. The observed phase velocities were compared with the theoretical phase velocities for existing  $V_s$  structures [Hatayama et al. (2007), AIST, and J-SHIS V2 models]. The phase velocity of the Hatayama et al. (2007) model which was estimated to simulate the 7–8 s period ground motions during the 2003 Tokachi-oki earthquake accurately explains the observed data (Fig. 8). Therefore, we inserted a 400 m/s layer (assuming the engineering bedrock) and used the  $V_s$  model of Hatayama et al. (2007) in the higher velocity part (over 400 m/s). Furthermore, we added a shallower layer to explain the 1-s period amplification referring, to the soil column of HKD126. These existing models are shown in Fig. 9. These  $V_s$  layer orders were used commonly for HKD126 and AOB and MKW01.

We estimated  $V_s$  by fitting selected phase velocities to the dispersion curve of the fundamental mode of the Rayleigh waves using the genetic algorithms inversion method (Yamanaka and Ishida 1996). We used

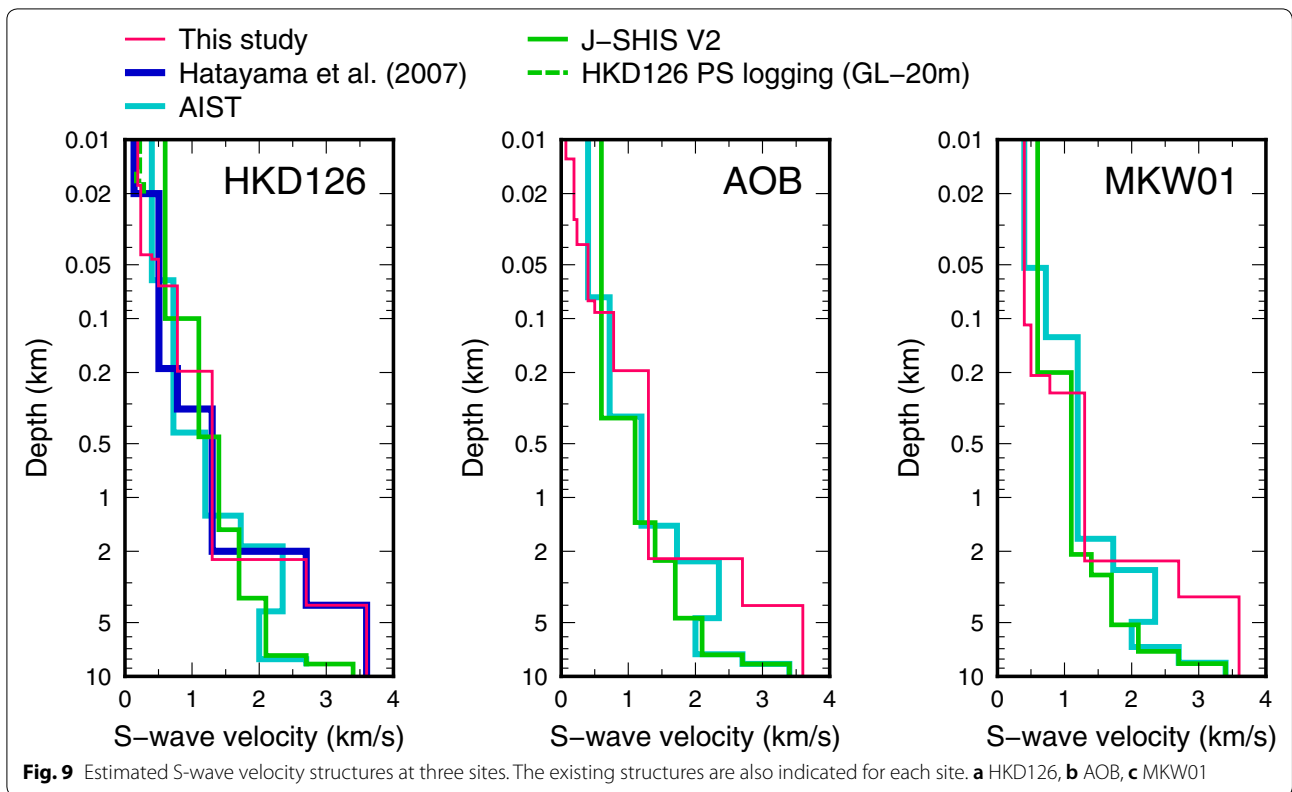
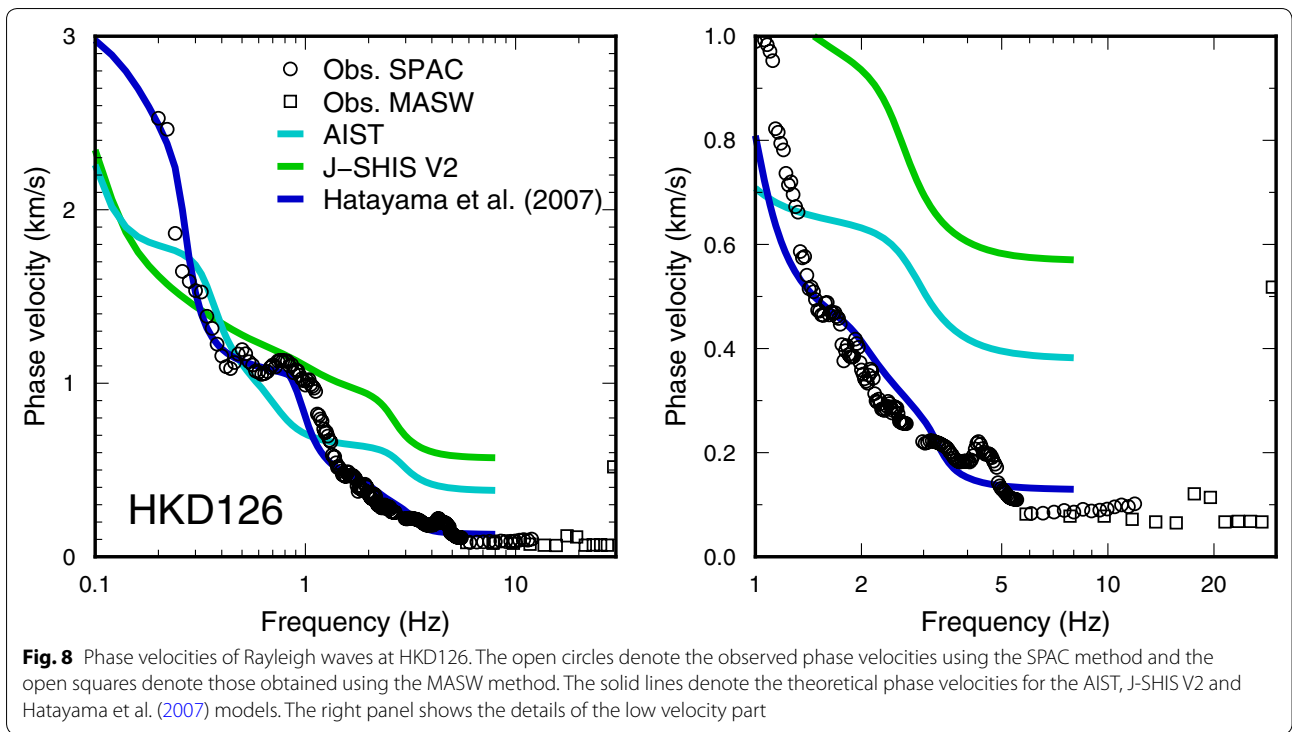


**Table 2 Search range for inversion**

$V_s$ (km/s)		Thickness (km)					
HKD126		HKD126		AOB		MKW01	
Low	High	Low	High	Low	High	Low	High
0.0500	0.0700	0.0070	0.0070	0.0100	0.0200	–	–
0.1000	0.2000	0.0110	0.0110	0.0100	0.0200	0.0090	0.0100
0.2000	0.3000	0.0260	0.0260	0.0100	0.0500	0.0800	0.1000
0.4000	0.4000	0.0010	0.1000	0.0100	0.1000	0.0900	0.1000
0.5000	0.5000	0.0100	0.3000	0.0100	0.1000	0.0500	0.1000
0.7800	0.7800	0.1000	0.5000	0.1000	0.2000	2.0000	2.1000
1.3000	1.3000	0.5000	3.0000	2.0000	2.1000	1.0000	2.0000
2.7000	2.7000	1.5000	3.0000	1.5000	2.0000	3.0000	3.5000
3.6000	3.6000	2.0000	5.0000	3.0000	3.5000	0.0090	0.0100

**Table 3 Estimated S-wave velocities and layer thickness at three sites**

$V_s$ (km/s)	Thickness (km)		
	HKD126	AOB	MKW01
0.070	0.007	0.013	–
0.191	0.011	0.015	0.017
0.234	0.026	0.011	0.010
0.400	0.003	0.041	0.082
0.500	0.020	0.013	0.090
0.780	0.131	0.103	0.054
1.300	2.023	2.003	2.000
2.700	1.781	1.820	1.469
3.600	–	–	–

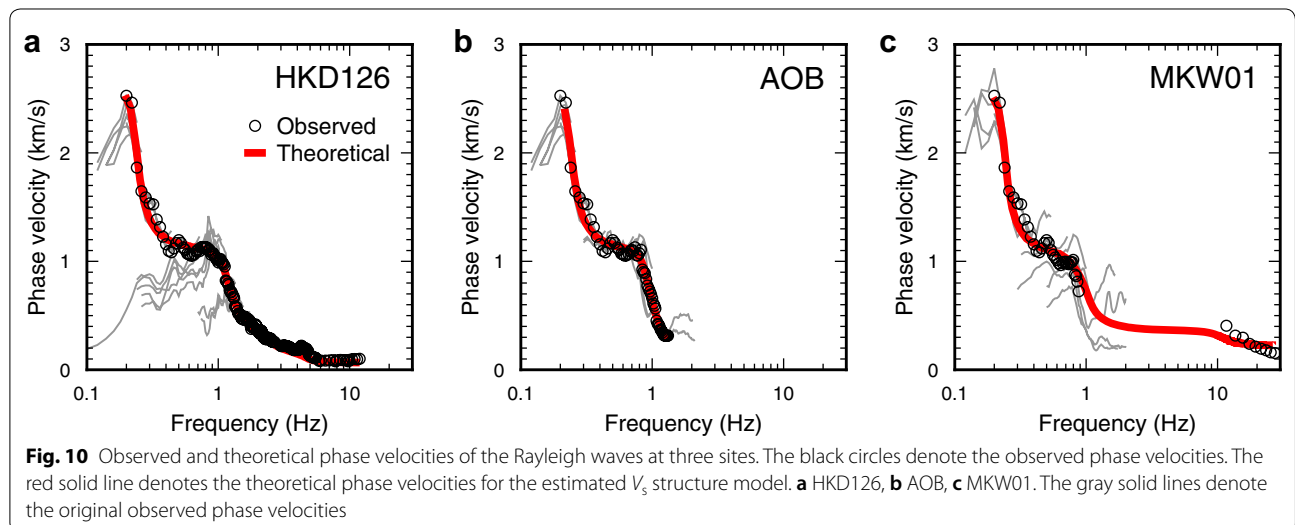
the following parameters in this method: the number of generations is 50, the population is 40, the crossover ratio is 70%, and the mutation ratio is 1%. The material

densities and P-wave velocities for each layer were estimated using the empirical relationship between them and the  $V_s$  obtained by Ludwig et al. (1970). The search range of the genetic algorithms is fixed as follows and shown in Table 2. For the deep part ( $V_s > 400$  m/s), the  $V_s$  values are fixed and the depth of the top of the 400 m/s layer was fixed with a hot spring drilling near HKD126 (Yamaguchi 1960; Oka 2004). For the shallower part, the thickness of each layer is fixed by the boundary of the soil column of HKD126 (Table 2).

**Results**

**HKD126**

The observed phase velocity and theoretical dispersion curve of the estimated  $V_s$  structure at HKD126 are compared in Fig. 10a and the estimated  $V_s$  structure is shown in Fig. 9a and Table 3. The theoretical dispersion curve well explains the observed value in the range of 0.2–10 Hz. The estimated  $V_s$  at the shallowest layer



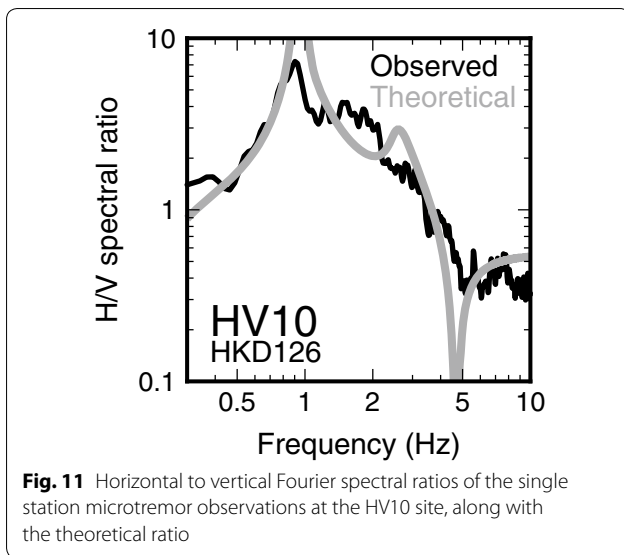


**Fig. 11** Horizontal to vertical Fourier spectral ratios of the single station microtremor observations at the HV10 site, along with the theoretical ratio

is 70 m/s, which is similar to the PS-logging data at HKD126 ( $V_s=60$  m/s). After constructing the  $V_s$  structure of HKD126, we used this structure to examine the other two sites.

**AOB**

AOB, the mid-point between HKD126 and MKW01, was selected on a flat plain, as HKD126 is located on a flat plain as well, to determine the variation. For the search range of  $V_s$  and thickness of each layer, we referred to from the HKD126 site. We selected AOB site to determine the variety of the engineering bedrock depth in the flat plain. We have not performed small SPAC and MASW methods around the AOB site because of the place for setting; therefore, the phase velocity is estimated to be less than 2 Hz. The observed phase velocities and theoretical dispersion curve of the estimated  $V_s$

structure at AOB are compared in Fig. 10b and the estimated  $V_s$  structure is shown in Fig. 9b and Table 3.

**MKW01**

Because the temporary station MKW01 site was on the hill (Fig. 5), it did not have a wide area to carry the wide SPAC arrays. The geomorphologic classification of MKW01 borders between terrace covered with volcanic ash soil and hill. We used phase velocities of the AOB large array ( $L$ : radius = 400 m) which was set on a lower flat field. The observed phase velocities of the arrays (radii = 120, 40 m) are connected to the those of the large array. Additionally, we used the phase velocity observed by MASW over 10 Hz. The phase velocities using the small SPAC array and the MASW converge to 200 m/s. Therefore, we removed two shallow layers ( $V_s=70$  m/s) from the estimated profile of HKD126 to invert the  $V_s$  structure. The observed phase velocities and the theoretical dispersion curve of the estimated  $V_s$  structure are compared in Fig. 10c and the estimated  $V_s$  structure is shown in Fig. 9c and Table 3.

Although there is no phase velocity of 1–10 Hz due to the problem of array size, theoretical dispersion curve and observed phase velocities correspond well in other frequency ranges (Fig. 10c).

**Single station microtremor linear array observation**

The single station microtremor observations were performed along the temporary strong motion high-density linear array (Fig. 5) using the same instruments that were employed for SPAC arrays.

The data processing for datasets was as follows. Each dataset were divided into 40.96 s windows tapered with a 5% cosine function. The Fourier spectra were smoothed using a 0.1 Hz Parzen window. The Fourier spectra of

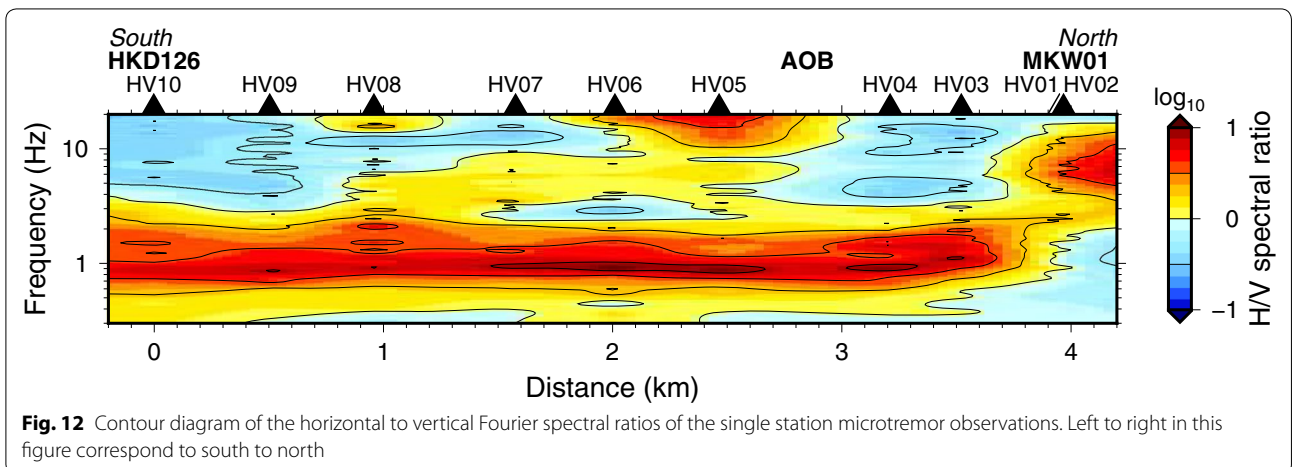


**Fig. 12** Contour diagram of the horizontal to vertical Fourier spectral ratios of the single station microtremor observations. Left to right in this figure correspond to south to north



the NS and EW component were averaged (root mean square) to obtain the horizontal component Fourier spectrum. Then the spectral ratios between the horizontal components and the vertical components were calculated. Finally, the spectral ratios of the horizontal component to the vertical component (H/V) were calculated using the arithmetic mean of 10 selected low noise sections. The H/V spectral ratio at HKD126 is shown in Fig. 11, along with the theoretical ratio of the constructed velocity structure. A contour diagram of the spectral ratio for the linear array is shown in Fig. 12. Their peak frequencies do not have large variations around 1 Hz in the flat plane area; however, a drastic change occurs near MKW01 in the frequency range of 1–10 Hz.

### Discussions

The constructed and existed structures are compared in Fig. 9 for each site. In Hatayama et al. (2007), the  $V_s = 1300$  m/s layer appears at a depth greater than 300 m; however, it appears within 200–300 m in the estimated  $V_s$  structures. This layer at HKD126 is shallower than the MKW01 layers, and the depth of the AOB layer lies in between. This tendency of the depth variation is the same as that of the seismic bedrock and the subsurface structure depth variation of the AIST and J-SHIS V2 models (Fig. 9). However, the similar value  $V_s$  layer of the J-SHIS V2 and AIST structures have many varieties (Fig. 9). Conversely, with respect to the shallow part, the engineering bedrock depth of MKW01 is shallower than that of HKD126. The seismic bedrock of AOB is at medium depth among the other sites; however, the surface soft soil deposit at AOB is detected to be thicker, down to about 13 m, than that at HKD126. The appearance of a second peak in the high-frequency range around HV05 matches these results (Fig. 12).

We have calculated the theoretical amplification factor of the SH-wave with the  $V_s$  structure, which was constructed as mentioned above (Fig. 13). We assumed that the input motion is a plane SH-wave at a depth of 1 km depth with an incident angle of  $0^\circ$ . The amplification factor of 1 Hz at AOB is the largest among the three sites. Further, the amplification factors of AOB and HKD126 are five times larger than that of MKW01 at a frequency of around 1 Hz. The reason for this tendency is the low  $V_s$  in the shallow part of the two sites; the engineering bedrock (400 m/s) of the two sites are deeper than that of MKW01.

We performed strong motion high-density linear array observation from December 1, 2018, to December 16, 2018, at six stations along the lines of HKD126 to MKW01 in Mukawa (Fig. 5) to investigate the variation of the strong ground motion in the target area. The

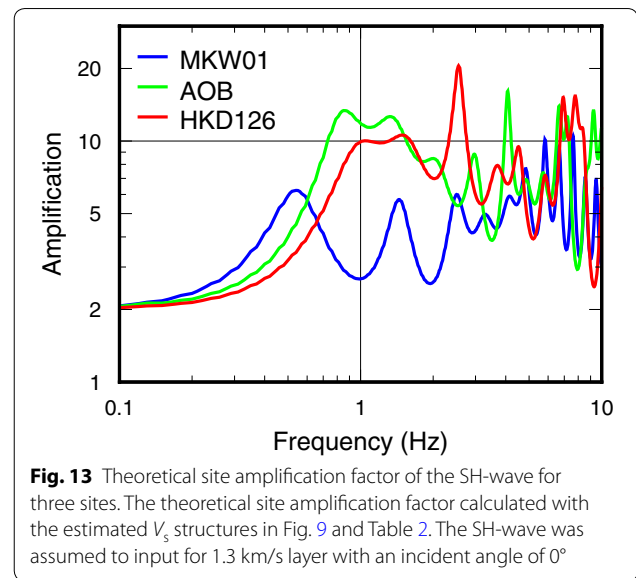


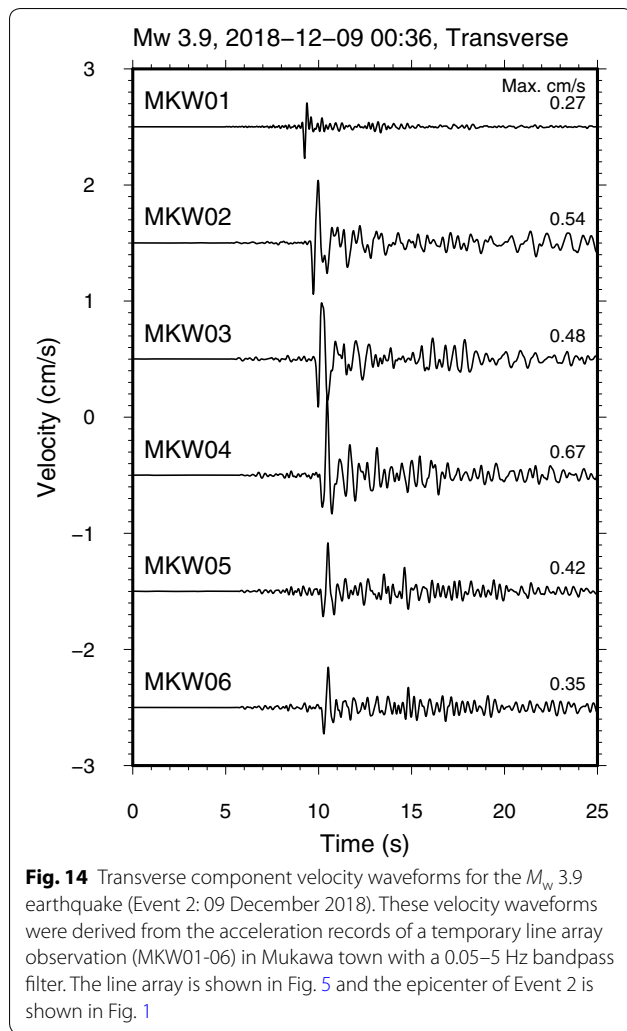
**Fig. 13** Theoretical site amplification factor of the SH-wave for three sites. The theoretical site amplification factor calculated with the estimated  $V_s$  structures in Fig. 9 and Table 2. The SH-wave was assumed to input for 1.3 km/s layer with an incident angle of  $0^\circ$

instruments used for this observation were the same as those for MKW01. The observed velocity waveforms of the transverse component during the aftershock (Event 2 in Fig. 1;  $M_w$  3.9, 9 December 2018) are shown in Fig. 14. The spectral ratios of the S-wave at the five stations were divided by the spectra at MKW01 (Fig. 15). These records were not affected by the nonlinear effect of soft soil, because their amplitudes were low.

As this study area is located in the collision zone, the deep crustal structure is complex (Miyamachi et al. 1994; Iwasaki et al. 2004) and the shape of the seismic bedrock is also complex (Hatayama et al. 2007). In the deep underground structures of the J-SHIS and AIST models, the seismic bedrock is slightly inclined to the northern side. The depth of the  $V_s = 1300$  m/s layer estimated in this study tends to incline to the north (Fig. 9). This may implicate the seismic bedrock variation in the deeper structure.

Among the observed spectral ratios of the five sites, the amplitudes of northern sites (MKW02, MKW03, MKW04) are larger than those of the southern sites (MKW05, MKW06) in the frequency range of 0.5–1 Hz. The theoretical spectral amplitudes in Fig. 13 are consistent with these observed spectral ratios. However, the amplitude of the observed spectral ratio of HKD126 (MKW05) is not larger than that of AOB (MKW02, 03). The cause of this difference between theory and observations might have to be discussed with other data (e.g., drilling data) in detail (Fig. 14).

The theoretical amplification factor of MKW01 is slightly larger than others at 0.3 Hz. We cannot recognize this phenomenon in the observed spectral ratios (Fig. 15); however, the spectral amplitude of MKW01 is larger than

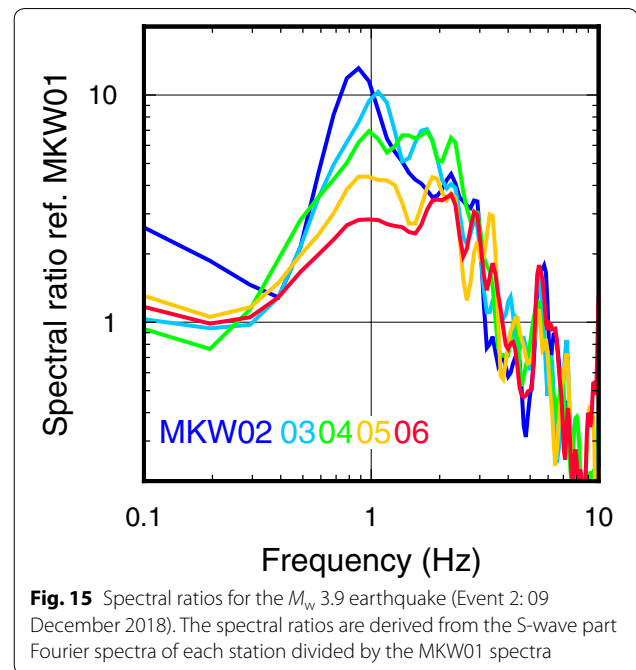


that of HKD126 at a frequency of approximately 0.3 Hz (Fig. 7). If we use the larger amplitude records, we can examine the effect of the seismic bedrock depth variation in detail. However, it is difficult to discuss this complex tendency through the results of our measurements.

The predominant periods during the main shock are longer than the predominant periods of theoretical and weak motion records (Fig. 4); this might be the effect of nonlinearity. The strong ground motion of the 1–2 s period during the main shock at HKD126 was mainly amplified by this shallow  $V_s$  structure, and this predominant range was shifted for long periods possibly due to the nonlinear effect.

### Concluding remarks

Severe building damage occurred around the HKD126 strong motion station during the 2018 Hokkaido eastern Iburī earthquake. This damage was caused by the 1–2 s ground motion which was the dominant period



in the velocity spectra. We conducted temporary strong motion, microtremor, and MASW observations in Mukawa town to investigate the underground structure. The estimated  $V_s$  structure that was inverted from the phase velocity using the microtremor array and MASW observations explained the strong ground motion characteristics during the main shock observed at HKD126. For the strong ground motion of the main shock, we confirmed that the shallow underground velocity structure was responsible for approximately 1 s at HKD126. For future studies, examining the nonlinear effect for HKD126 in detail is important. To do this, we must consider more ground motion records from a wider area for obtaining a detailed three-dimensional velocity structure.

### Abbreviations

AIST: National Institute of Advanced Industrial Science and Technology; DNL: degree of nonlinearity; H/V: horizontal component divided by vertical component; JMA: Japan Meteorological Agency; J-SHIS: Japan Seismic Hazard Information Station; JST: Japan Standard Time; KiK-net: Kiban Kyoshin network; K-NET: Kyoshin network;  $M_{JMA}$ : JMA magnitude;  $M_w$ : moment magnitude; NIED: National Research Institute for Earth Science and Disaster Resilience; SPAC: spatial autocorrelation;  $V_s$ : shear wave (S-wave) velocity;  $AVS_{30}$ : average S-wave velocity in the upper 30 m of the soil layer.

### Acknowledgements

We thank the Japan Meteorological Agency (JMA), National Research Institute for Earth Science and Disaster Resilience (NIED), Railway Technical Research Institute (RTRI) and National Institute of Advanced Industrial Science and Technology (AIST) for providing us with the hypocenter information, underground structure, and strong motion data. We used the Generic Mapping Tools (Wessel et al. 2013) for drawing the parts of the figures. Further, we thank Dr. Bijkuchhen Subeg and Dr. Kim Yong Cheol, who joined in the observations. We appreciate Dr. Takuji Yamada, Dr. Tomoko Elizabeth Yano and two

anonymous reviewers for their constructive comments, which improved the manuscript significantly.

#### Authors' contributions

NT and MS designed this study. NT, MS, HT, TM, MI, and ST planned and installed the temporary strong motion observations. NT, MS, JH, SN, TM, HY, KC, ST, MK, and NY performed the microtremor and MASW measurements. NT drafted the manuscript. All authors read and approved the final manuscript.

#### Funding

This study was partly supported by the Grant-in-Aid for Scientific Research Nos. 18K19952, 16K16370, 16K06586 and 17H06215 from MEXT of Japan, Core-to-Core collaborative Research 2018 at ERI and DPRI, and MEXT of Japan's Earthquake and Volcano Hazards Observation and Research Program.

#### Availability of data and materials

The strong motion (K-NET and KiK-net) recordings and PS loggings used in this study were downloaded from the websites: <http://www.kyoshin.bosai.go.jp/>. The moment magnitude was taken from the website: <http://www.fnet.bosai.go.jp/event/joho.php?LANG=en>. The strong motion recordings at the JMA sites were downloaded in Japanese from [https://www.data.jma.go.jp/svd/eww/data/ltpgm\\_explain/data/past/20180906030805/index.html](https://www.data.jma.go.jp/svd/eww/data/ltpgm_explain/data/past/20180906030805/index.html). The hypocenter, moment magnitude, and focal mechanism information plotted in Fig. 1 were taken from the website: <http://www.fnet.bosai.go.jp/event/joho.php?LANG=en>. The base map of Fig. 5 was obtained from obtained from the geospatial information authority of Japan (GSI).

#### Ethics approval and consent to participate

Not applicable.

#### Consent for publication

Not applicable.

#### Competing interests

The authors declare that they have no competing interests.

#### Author details

<sup>1</sup> Hokkaido University, Kita 13, Nishi 8, Kita-ku, Sapporo, Hokkaido, Japan. <sup>2</sup> Kyushu University, Motoooka 744, Nishi-ku, Fukuoka, Japan. <sup>3</sup> Geo-Technical Research Co., Ltd, Atsubetsu Higashi 5-1-4-6, Atsubetsu-ku, Sapporo, Hokkaido, Japan. <sup>4</sup> National Research Institute for Earth Science and Disaster Resilience, 3-1 Tennodai, Tsukuba, Ibaraki, Japan. <sup>5</sup> Institute of Seismology and Volcanology, Hokkaido University, Kita 10, Nishi 8, Kita-ku, Sapporo, Japan. <sup>6</sup> Tokyo Institute of Technology, 4259 Nagatsuta, Midori-ku Yokohama, Kanagawa, Japan. <sup>7</sup> Railway Technical Research Institute, 2-8-38 Hikari-cho, Kokubunji, Tokyo, Japan. <sup>8</sup> Kochi University, 2-5-1, Akebono-cho, Kochi, Kochi, Japan.

Received: 5 March 2019 Accepted: 24 May 2019

Published online: 13 June 2019

#### References

- Fujiwara H, Kawai S, Aoi S, Morikawa N, Senna S, Azuma H, Ooi M, Hao K, Hasegawa N, Maeda T (2012) Some improvements of seismic hazard assessment based on the 2011 Tohoku earthquake. *Tech Note Natl Res Inst Earth Sci Disaster Prev* 379:1–349
- Hatayama K, Kanno T, Kudo K (2007) Control factors of spatial variation of long-period strong ground motions in the Yufutsu sedimentary basin, Hokkaido, during the Mw 8.0 2003 Tokachi-oki, Japan, Earthquake. *Bull Seismol Soc Am* 97(4):1308–1323. <https://doi.org/10.1785/0120060200>
- Iwasaki T, Adachi K, Moriya T, Miyamachi H, Matsushima T, Miyashita K, Takeda T, Taira T, Yamada T, Ohtake K (2004) Upper and middle crustal deformation of an arc–arc collision across Hokkaido, Japan, inferred from seismic refraction/wide-angle reflection experiments. *Tectonophysics* 388(1):59–73. <https://doi.org/10.1016/j.tecto.2004.03.025>
- Kawase H (1996) The cause of the damage belt in Kobe: “the basin-edge effect”, constructive interference of the direct S-wave with the basin-induced diffracted/Rayleigh waves. *Seismol Res Lett* 67(5):25–34. <https://doi.org/10.1785/gssrl.67.5.25>

- Ludwig WJ, Nafe JE, Drake CL (1970) Seismic refraction. In: Maxwell AE (ed) *The sea*, vol 4. Wiley, New York, pp 53–84
- Miyamachi H, Kasahara M, Suzuki S, Tanaka K, Hasegawa A (1994) Seismic velocity structure in the crust and upper mantle beneath Northern Japan. *J Phys Earth* 42(4):269–301. <https://doi.org/10.4294/jpe1952.42.269>
- Nakamura Y, Uehara F, Inoue H (1996) Waveform and its analysis of the 1995 Hyogo-Ken-Nanbu Earthquake (II). *JR Earthquake Information No. 23d*, Railway Technical Research Institute (in Japanese)
- Noguchi S, Sasatani T (2008) Quantification of degree of nonlinear site response. In: *The 14th world conference on earthquake engineering*, Beijing, China
- Noguchi S, Sato H, Sasatani T (2016) Evaluation of nonlinear soil response during the 2011 off the Pacific coast of Tohoku earthquake by means of a simple index of soil nonlinearity. *J Jpn Assoc Earthq Eng* 16(4):4\_93–94\_105. [https://doi.org/10.5610/jaee.16.4\\_93](https://doi.org/10.5610/jaee.16.4_93)
- Oka T (2004) Analyzing the subsurface geologic structure of Tomakomai region by drilling data of fluid resources, in connection with the earthquake motion of the Tokachi-oki Earthquake in 2003. *Rep Geol Surv Hokkaido* 75:85–108
- Okada H (2003) The microtremor survey method. *Geophysical monograph series no. 12*. Tulsa. <https://doi.org/10.1190/1.9781560801740>
- Park CB, Miller RD, Xia J (1999) Multichannel analysis of surface waves. *Geophysics* 64(3):800–808. <https://doi.org/10.1190/1.1444590>
- Sakai Y, Kanno T, Koketsu K (2004) Proposal of instrumental seismic intensity scale from response spectra in various period ranges. *J Struct Constr Eng* 585:71–76
- The Headquarters for Earthquake Research Promotion (2018) Japan seismic hazard information station ver. 2018. <http://www.j-shis.bosai.go.jp/map/>. Accessed 19 Feb 2019
- Wessel P, Smith WHF, Scharroo R, Luis J, Wobbe F (2013) Generic mapping tools: improved version released. *Eos Trans Am Geophys Union* 94(45):409–410
- Yamaguchi S (1960) Mukawa (explanatory text of the geological map of Japan). Geological Survey of Japan, Tsukuba
- Yamanaka H, Ishida H (1996) Application of genetic algorithms to an inversion of surface-wave dispersion data. *Bull Seismol Soc Am* 86(2):436–444
- Yoshida K, Yoshimi M, Suzuki H, Morino M, Takizawa F, Sekiguchi H, Horikawa H (2007) 3D velocity structure model of the Ishikari and Yufutsu sedimentary basins. *Annual report on active fault and paleoearthquake research no. 7*, pp 1–29

#### Publisher's Note

Springer Nature remains neutral with regard to jurisdictional claims in published maps and institutional affiliations.

Submit your manuscript to a SpringerOpen® journal and benefit from:

- Convenient online submission
- Rigorous peer review
- Open access: articles freely available online
- High visibility within the field
- Retaining the copyright to your article

Submit your next manuscript at ► [springeropen.com](http://springeropen.com)